BIOCHEMISTRY
including biophysical chemistry & molecular biology

Folding Dynamics and Pathways of the Trp-Cage Miniproteins

Aimee Byrne,[†] D. Victoria Williams,[†] Bipasha Barua,[†] Stephen J. Hagen,[‡] Brandon L. Kier,[†] and Niels H. Andersen*,[†]

[†]Department of Chemistry, University of Washington, Seattle, Washington 98195, United States
[‡]Physics Department, University of Florida, Gainesville, Florida 32611, United States

Ⓢ Supporting Information

ABSTRACT: Using alternate measures of fold stability for a wide variety of Trp-cage mutants has raised the possibility that prior dynamics T-jump measures may not be reporting on complete cage formation for some species. NMR relaxation studies using probes that only achieve large chemical shift difference from unfolded values on complete cage formation indicate slower folding in some but not all cases. Fourteen species have been examined, with cage formation time constants ($1/k_F$) ranging from 0.9–7.5 μs at 300 K. The present study does not change the status of the Trp-cage as a fast folding, essentially two-state system, although it does alter the stage at which this description applies. A diversity of prestructuring events, depending on the specific analogue examined, may appear in the folding scenario, but in all cases, formation of the N-terminal helix is complete either at or before the cage-formation transition state. In contrast, the fold-stabilizing H-bonding interactions of the buried Ser14 side chain and the Arg/Asp salt bridge are post-transition state features on the folding pathway. The study has also found instances in which a [P12W] mutation is fold destabilizing but still serves to accelerate the folding process.

Fast Folding Without a Salt Bridge
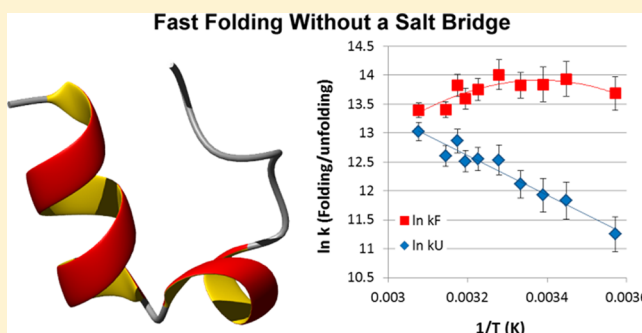
The Trp-cage has become a protein folding paradigm and the preferred test system for molecular dynamics (MD) based folding studies and fold prediction algorithms.[1,2] The two features that led to this status are its small size and fast folding rates. A wide variety of folding pathways have been proposed based on these computational studies, and quite different conclusions have been reached concerning the extent to which this model protein should be viewed as an unfolded ensemble proceeding to a fully folded state with no detectable intermediates. Turning to the experimental data, the fast folding of the Trp-cage (the original TC5b construct, NLYIQ WLKDG GPSSG RPPPS, T_m = 42 °C) was noted in the very first report on the fold,[3] there given as $1/k_F$ = 7 ± 2 μs at 40 °C based on both NMR exchange broadening and IR-monitored T-jump experiments. The NMR experiment employed a G11α resonance which has a 3.5 ppm upfield ring current shift as the probe. The T-jump experiment followed the decrease in the "solvated" helical amide I′ band (1628 cm^{-1}) amplitude after a 10 °C T-jump which fit to a single exponential.

With the 2002 publication of the details regarding the characterization of TC5b,[4] the system attracted the attention of other biophysicists. Because of the extreme quenching of Trp fluorescence associated with the folded state,[5] fluorescence-monitored T-jump experiments were another possibility. Qiu et al.[6] reported $1/k_F$ = 4.1 μs at 23.5 °C with the published data graph indicating a folding time constant of 3.56 μs at 300 K. In 2011, the Gai lab[7] reported essentially the same value in T-

jump experiments monitoring the helical amide band (specifically at 1630 cm^{-1}), $1/k_F$ = 3.7 μs at 25 °C.

Culik et al.[7] also reported dynamics data for TC10b, a sequence (DAYAQ WLKDG GPSSG RPPPS, T_m = 56 °C[8] that forms a more stable Trp-cage fold largely due to the enhanced intrinsic helicity[9] of the residue Asp1−Lys8 span. Culik et al. employed the DA*YA*QW··· sequence with A* = ^{13}C′-Ala and observed peaks at 1586, 1615, and 1646 (all with decreasing absorbance on warming) and 1664−1672 cm^{-1} (increasing absorbance on warming) in the temperature-differenced FT-IR spectra. These were attributed to 1586 (the Asp-CO$_2^-$ signal in the salt bridge), 1615 (helical A*), 1646 (a shifted unlabeled helical amide band, shifted due to an overlapping nonhelical A* peak), and 1664 cm^{-1} (a 3_{10} helix signal and an increasing random coil signal). These assignments may not be correct. The effect of ^{13}C=O labeling is expected to be a 36 cm^{-1} frequency shift versus ^{12}C=O and has been measured[10] at 39 cm^{-1} in model helices. There was a distinct maximum at 1630 cm^{-1} separating the 1615 and 1646 minima in the FT-IR difference spectra reported by Culik et al.[7] We would attribute the 1630 maximum to increases in random coil A* and would expect the negative peak at 1586 to contain a significant component of helical-A* melting. Gai and co-workers
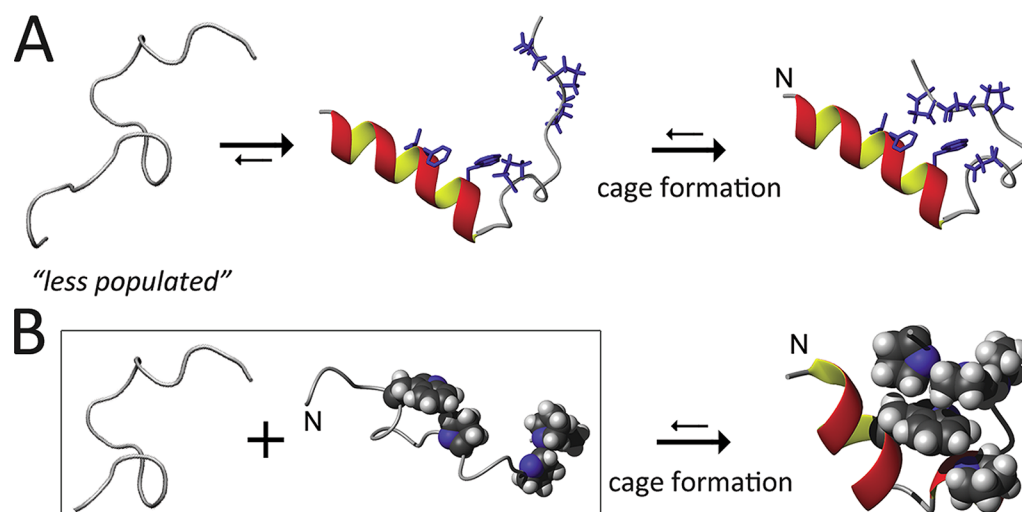
Figure 1. Half-cage structures, with no ring current shifts at P18 and no sequestration of the Trp indole side chain NH, have interactions between W6 and the G11-P12 unit which result in upfield ring current shifts in those residues that are not the same as those in the complete cage structure. Postulated half-cage structures of Trp-cage-forming sequences have either (A) a fully formed N-terminal helix with the W6/P12 interactions as a helix C-cap (illustrated with a long helix such as that in exendin-4 and earlier incomplete truncation species[4,18]) or (B) represent transient interactions within the unfolded ensemble that may or may not be on-path to the full cage structure. Scenario B was first suggested for TC5b.[4]

monitored relaxation after the T-jumps at 1580, 1612, and 1664 cm^{-1}. At 1664 cm^{-1}, the data were biexponential with the following time constants at 292 K, τ = 300 ns (attributed to local unfolding of the 3_{10} helix) and τ = 2.5 μs (growth of unlabeled random coil ^{12}C=O). The slow phase was attributed to global unfolding and gave the same time constants observed as when monitoring at 1580 or 1612 cm^{-1}: $1/k_F$ = 1.55 μs at 25 °C.

Pertinent to the present study, the Feng Gai group has also measured the effects of a number of mutations on folding dynamics. These included the Gly10 to D-Ala mutation which we reported in 2008[11] as a strategy for creating hyperstable Trp-cages. Culik et al.[12] reported that the fold-stabilizing G10a mutation (ΔT_m = +21 °C) increased the folding rate of TC5b by only a factor of 2. Two additional mutations, R16K and P19A, were examined in the case of TC10b,[7] and neither was reported to alter the folding rate appreciably. The P19A mutation is a particularly destabilizing mutation, ΔT_m = −44 °C, as quoted by Culik et al.[7] As a result, Feng Gai and co-workers have proposed that hydrophobic staple (Y3/P19) and salt-bridge (D9/R16) formation occur on the downhill side of the folding transition and only stabilize the final state; essentially, that helix formation is rate determining and sets the stage for downhill folding events thereafter.

The Arrhenius plots for all Trp-cage dynamics studies mentioned to this point indicate faster folding rates on warming (a negative Arrhenius plot slope). Although the slopes for folding were always less than slopes for the unfolding process, positive folding E_a values were observed throughout. The one exception to this is an early study of another stabilizing mutation, [P12W], which introduces an additional aryl/aryl interaction and results in more apolar burial. Bunagan et al.[13] reported dynamics data for [P12W]-TC5b, T_m = 57 °C, which are considerably more protein-like (vide infra): a curved plot for log k_F versus $1/T$ with an increasingly negative E_a at temperatures well below T_m. Positive Arrhenius slopes (negative E_a values) usually indicate a compact transition state with hydrophobic surface burial. The [P12W] mutation also provided the first notable instance of folding rate

acceleration, $1/k_F$ about 1 μs at 300 K—corresponding to a 3.5-fold acceleration. Subsequent studies have shown that P12W is a stabilizing mutation in other Trp-cage species.[14]

With the exception of the study reported by Qiu et al.,[6] all previous T-jump studies of Trp-cage dynamics have relied on the disappearance of helical amide I′ bands, either monitored directly or as the appearance of a random coil amide absorbance. We view this as a potential source of error in assessing the rates at which a fully formed Trp-cage fold appears. There have been several reports[8,15] that suggest that the N-terminal helix is partially retained in unfolded state ensembles or is a very early on-path state along MD folding trajectories.[1c,16] Indeed, we have proposed the existence of half-cage species (Figure 1), either as intermediates or as partially folded species within the "unfolded ensemble".[4,8,17] In the case of exendin-4, which has a much longer and thus more stable α helix, the unfolded state in aqueous fluoroalcohol media has a fully formed helix with cage formation occurring as a separate docking event (scenario A, Figure 1).

In the case of Trp-cage species with stabilizing mutations in the α helical segment, an intermediate situation, between A and B of Figure 1, may apply (vide infra). In support of this scheme, half-cage structures with an upfield G11-CH$_2$ group appear to be present within the unfolded ensemble of TC5b and other less stable Trp-cage analogues.[4,8,14] Long-range W6/P12 and W6/R16 contacts have been identified[17] in the unfolded state of TC5b.[19] In another study,[19] it was noted that W6/R16 NOEs are retained at and slightly above the T_m to a greater extent than other long-range contacts.

In our 2008 report on the [P19A] mutant of TC10b,[8] we noted this species as an example in which different probes give radically different T_m data. The CD melt as well as chemical shift melts for the Hα protons in the N-terminal helix yielded a T_m of 15 °C. However, the NMR shifts for the ring-current shifted Hα and Hβ3 sites in Pro18 indicated a fold population (χ_F) of only 0.17 at 280 K and an extrapolated Tm below −9 °C. On this basis, the $\Delta\Delta G_F$ value for complete cage formation associated with the P19A mutation is at least 11 kJ/mol, with our best estimate at 14 kJ/mol. As a result, we were surprised

by the report[7] that [P19A]-TC10b folds as rapidly as the nonmutated sequence; in our view, it raised the possibility that all previous Trp-cage folding dynamics may represent just helix formation, not cage formation.

Herein we report our efforts to find dynamics probes that exclusively reflect the formation of the complete cage structure and the application of these to determine which structure-stabilizing features of the Trp-cage are present at this folding transition state and which form after the transition state. Throughout, we have relied primarily on NMR resonances that display very large structuring shifts due to ring-current effects that are present only when the complete cage structure forms. As expected,[20,21] these highly shifted resonances display measurable line broadening when in equilibrium with a significant unfolded state population.

■ MATERIALS AND METHODS

Peptide Synthesis and Characterization. Many of the systems examined herein, or used for the evaluation of mutational $\Delta\Delta G$-values, have been reported previously,[8,11,14,15] and the others were prepared in the same way (automated FMOC-based peptide synthesis) and similarly purified and characterized by NMR spectroscopy and circular dichroism (CD) melts. All of the new Trp-cage analogues in this report displayed the expected $(M + 2H)^{+2}$ and $(M + 3H)^{+3}$ molecular ions by electrospray mass spectrometry (Bruker Esquire Ion Trap). In addition, all species with ΔG_U values greater than −2 displayed the diagnostic long-range NOEs and the upfield shifts at G11Hα2, P18Hα, Hβ3 (or A18Hα and Hβ), and L7Hα as well as downfield shifts at R16 proton sites that reflect Trp-cage fold formation.[8,14,15] The complete list, including reference compounds, appears in Table 1. All ΔG_U values have been recalculated based on the structuring shifts, expressed as chemical shift deviations (CSDs, the observed shift minus the coil reference value) at residue 18 so as to reflect complete cage structure formation rather than helix content. In contrast, CD measures and the resulting T_m values from the melting curve reflect only loss of helicity.

NMR Relaxation Methods for Obtaining Folding Dynamics. The dynamics data obtained at U.W. are based on NMR resonance line broadening associated with exchange between the folded state and a populated unfolded state which lacks the structuring shifts associated with fold formation.[20,21] For most of the studies reported herein, this analysis assumes a two-state equilibrium between a fully folded cage state and an unfolded ensemble that has no structuring shifts for the probes examined—proton sites at residue 18 in an undocked polyPro$_{II}$ unit.

For the few studies based on line broadening at the G11Hα2 site (panel A of Figure 2, Figure 4, and Table 2, vide infra), we needed to take into account the presence of half-cage species in the precage unfolded ensemble. A half-cage model (see Figure 1, vide supra) was required to obtain expectation chemical shifts for G11Hα2 at different temperatures in both water and water/trifluoroethanol (TFE) mixtures. Our chosen model for incomplete cage formation was the NAUYU QWLKD GGPSS GRP<u>AA</u> sequence.[22] The N-terminal changes, including two helix-favoring Aib residues (U in the sequence shown) are favorable for helix and half-cage formation, while the Ala substitution for two C-terminal prolines compromises full cage formation. NAUYU QWLKD GGPSS GRP<u>PPS</u>,[8] which lacks the C-terminal changes displays helix (CD) and cage melting points that are nearly the same: 59 and 53.5 °C, respectively. In

the case of NAUYU QWLKD GGPSS GRP<u>AA</u> (CD T_m = 23 °C), helix and half-cage formation occurs. From Table 1, the

Table 1. Structure Designations,[a] Sequences, and Fold Stability Data[b] for Key Trp-Cage Variants and Their Single Site Residue Mutants[c]

Desig.	Sequence	Tm (CD)	ΔG_U^{300K}	ΔG_U^{320K}
TC12b [8]	NYAQWLKDGGPSSGRPPPS	36	1.3	
TC11b1 [8]	GAYAQWLKDGGPSSGRPPPS	40	2.4	
TC9b [8]	NAYAQWLKDGGPSSGRPPPS	51	4.4	
at pH 2.5		39	1.1[5]	
[R16nva]- [8]		36	0.6	
Control [22]	NAUYUQWLKDGGPSSGRPAA	**23**	**−5.6**	
TC10b [8]	DAYAQWLKDGGPSSGRPPPS	56	5.3[5]	1.5
at pH 2.5		41	1.6[5]	−1.5
[P19A]- [8]		**15**	**−6.5**	
[S14A]- [8]		21	−0.7	−3.9[5]
[P17A]- [8]		46	2.6	-0.6[5]
[P18A]- [8]		47	4.3	0.0
[P12W,P18A]-		40	1.9	−2.3[5]
TC13b [12]	DAYAQWLADGGPASGRPPPS	68	6.3	2.9[5]
[P12W]- [14]		77	9.2[5]	5.3
[P12W,P18A]		59	5.2	0.9
at pH 2.5		49.5	2.1	−1.2
add P17A pH 7		n.d.	3.3[5]	−0.3
tr-TC16b	Ac-AYAQWLAD**a**GPAS**a**RPPPS	68	8.1[5]	6.7
at pH 2.5		60	5.4[5]	
[R16nva]-		49.5	2.1	−0.2
TC16b [11]	DAYAQWLAD**a**GPAS**a**RPPPS	83	10.2	7.0
at pH 2.5 [14]		74	5.7	3.5
[P12W]- [14]		97	≥ 11.7	8.4[5]
[R16nva]-		63	2.6	−0.1
[P19A]-		**43**	**−1.5**	
[P18A]		76	8.9	∼ 4.7
at pH 2.5		n.d.	5.8	1.9
add [P17A]		64	6.4	3.1
at pH 2.5		n.d.	3.3	
add [R16nva]		n.d.	4.0[5]	1.7
add [P12W]		64	7.6	3.8[5]
add [A8G]		52	4.8	1.1
at pH 2.5		42.5	2.3	−1.0
add [S14A]		55.5	3.6	2.2
at pH 2.5		38.5	0.5	−1.8[5]
add [S14A,P12W]		51	1.9	−0.64
at pH 2.5		**39**	**−0.4**	

[a]The structure designations and the first citation for each species are given. Sequences or conditions without a citation are new reports in this account. The ΔG_U values are calculated, or recalculated, as indicated[c]and do not correspond in all cases to those previously reported, particularly in cases where the previous report was based on CD monitored melting. The most extreme cases are highlighted in a larger bold font. [b]The ΔG_U values (in kJ/mol, given to nearest 0.05 kJ) are −ΔG_F with this reflecting "complete cage formation". The decrease in the CSDs of the P18 Hα and Hβ3 (or, for [P18A] mutants, the A18 Hα and Hβ) resonances from either the reference values for the fully folded state, or from the observed 280 K values when T_m(CD) > 80 °C, are used to obtain the fraction folded (χ_{cage}) value at the higher temperatures. A 1%/10 °C decrease in the fully folded CSD on warming is assumed. The observed CSD temperature gradients (which are linear) for extreme ring-current-shifted sites of hyperstable (T_m > 90 °C) cyclic constructs[23] have varied from 0.070 to 0.145%/°C in the 290−320 K temperature range. [c]Bold data indicate large differences between the CD and NMR measures of fold stability.

$\Delta\Delta G_U$ values for P19A and P18A are −11.8 and ca. −1.2 kJ/mol, respectively. The fractional population of the complete cage structure (χ_{cage}) for this model based on the ring current shift observed at A18α (2.69 ppm upfield in [P18A]-TC16a at 280 K) is 0.20 (280 K), 0.15 (290 K), 0.094 (300 K), and 0.056 (310 K) in pH 7 aqueous buffer. With the addition of TFE to 30 vol %, the χ_{cage}-value increases to 0.33 at 280 K (and 0.11 at 310 K). These results allowed us to calculate expectation
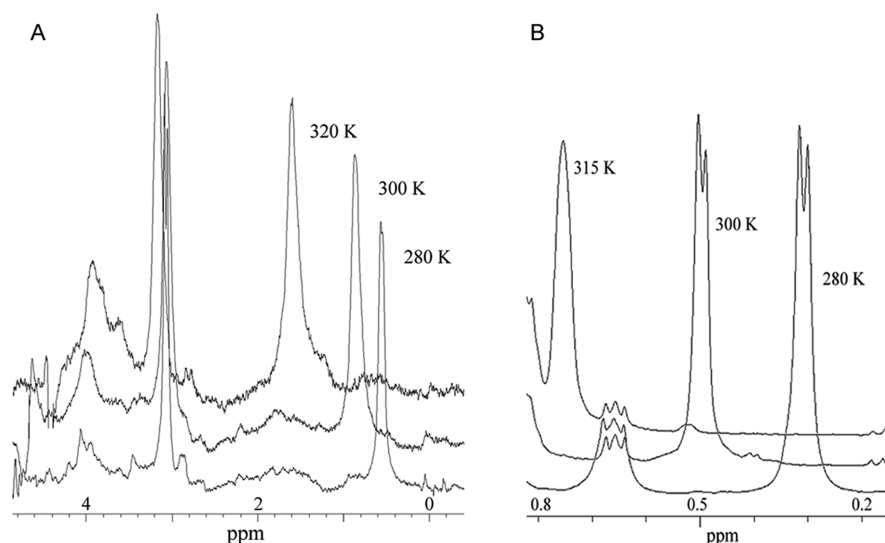
Figure 2. (A) The ^{13}C-edited spectra of [G11-^{13}Cα]-TC10b at three temperatures. Note the greater broadening of the upfield Hα signal and the extent to which it shifts to higher δ values on warming. In contrast, the downfield G11Hα shows much less broadening and hardly shifts on warming. (B) The upfield region of the spectrum of [P18A]-TC10b at three temperature showing the unfolding-induced shift and line width changes for the Ala-18-Hβ signal. The three-line signal at 0.66 ppm is a −C$\underline{H}$D-SiMe$_3$ unit in the added chemical shift standard.

11Hα2 shifts from the observed values for the ensemble containing small amounts of the fully folded species. To correct the observed G11Hα2 δ-values to those due to the "pre-cage ensemble" including a partially populated half-cage, we assumed that the full-cage species would display the usual far upfield shift, given by $\delta = 0.488 + 0.0036$ (T-280) ppm.

The two types of NMR line width data employed are illustrated for TC10b and its [P18A]-analogue in Figure 2.

The excess broadening observed for the probes is equated with Δ^{ex} and eq 1[20,21,24] is used to calculate the value of k_F at each temperature.

$$K_F = 4\pi\chi_U(\chi_F)^2(\Delta\nu)^2(\Delta^{ex})^{-1} \qquad (1)$$

The values of χ_F and χ_U $(= 1 - \chi_F)$ are obtained from the CSD of the probe: $\chi_F = \mathrm{CSD}^{obs}/\mathrm{CSD}^{100\%}$. The $\Delta\nu$ in eq 1 is given as the CSD$^{100\%}$ and has a small temperature dependence (see Table 1). The k_U value at each temperature is calculated as $k_U = k_F(1 - \chi_F)(\chi_F)^{-1}$.

In the case of [G11-^{13}Cα]-Trp-cage species, the excess broadening at G11Hα2 (versus G11Hα3) was analyzed based on several models as described in the Ph.D. thesis of Barua.[22] The model using the expectation shifts from the NAUYU QWLKD GGPSS GRPAA sequence half-cage model (vide supra) affords rates that are, within experimental error, in agreement with fluorescence-monitored T-jump studies (Figure 4) and IR-monitored T-jump studies subsequently reported by Culik et al.[7] In Figure 4, the errors in the ln k_F values from the fluorescence-monitored T-jump study vary from ±0.07 to ±0.17. Our best estimates of the error in both folding rates from the NMR experiment are also included on the graph. Assuming a random coil shift for G11Hα2 in the "unfolded state" affords a folding rate that is faster by a factor of 1.6. As a result, the same analysis using the G11Hα2 reference shifts from the half-cage model was employed for the other [G11-^{13}Cα]-TC species examined.

In the case of dynamics studies based on the alanine-CH$_3$ signal of [P18A]-analogues, the increase in line width of this signal is the measure that affords dynamics data; the chemical shift provides the equilibrium constant at each temperature.
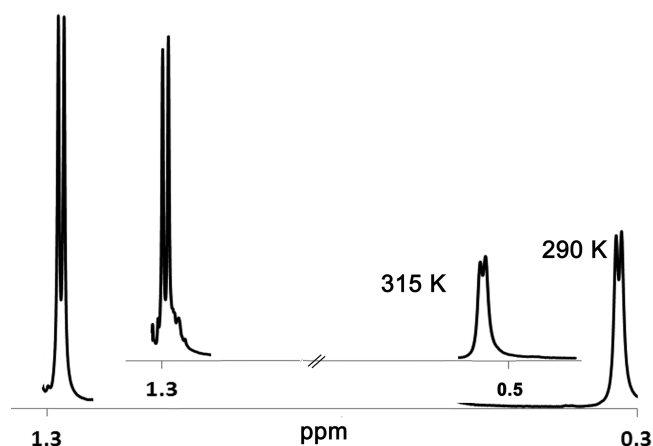

Figure 3. Two segments of the upfield spectrum of [A8G,P18A]-TC16b at 290 and 315 K. Line shape fitting of the peak at 1.28 ppm, due to D-Ala10β, which appears quite close to the coil reference shift (1.39 ppm) for Ala-Hβ and shifts less than 0.03 ppm over a 40 °C range, provides the intrinsic line width parameter ($\Delta°$) for the experiment. The line width increment due to exchange broadening results in a wider A18β peak with less separation, %-dip,[20,21] between the two lines of the doublet.

The 100% folded values for this signal, taken from the most stable Trp-cage analogues with this mutation, are 0.25 ppm (CSD = −1.14 ppm) and 0.20 ppm (CSD = −1.19 ± 0.005 ppm), respectively, for species with and without a P12W substitution. The sensitivity of alanine-CH$_3$ resonances to quite small Δ^{ex} terms is illustrated in Figure 3.

In a typical experiment, the line width at half height is measured for two or three well-resolved alanine methyls that appear within 0.15 ppm of the random coil value when in the folded state. A high and low value for Δ^{ex} is determined by direct half height width comparisons to these references. Two additional values for Δ^{ex} are obtained by modeling the A18β line shape in a custom built Excel spreadsheet using the A18β coupling constant measured at the lowest temperature and varying the line width (Δ^{sim}) until the observed half height
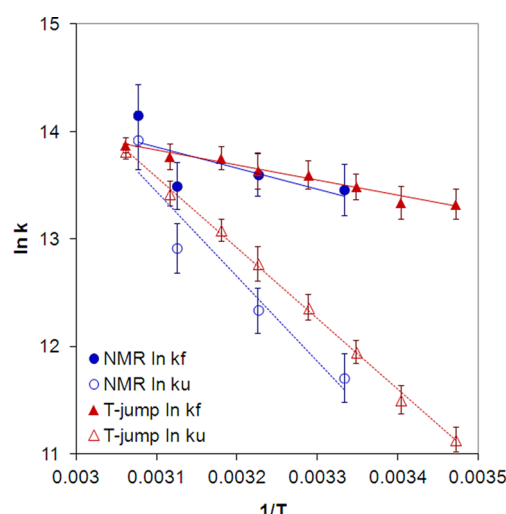
Figure 4. A comparison of Arrhenius plots for TC10b obtained in a fluorescence-monitored T-jump experiment and from H11α2 linewidths.
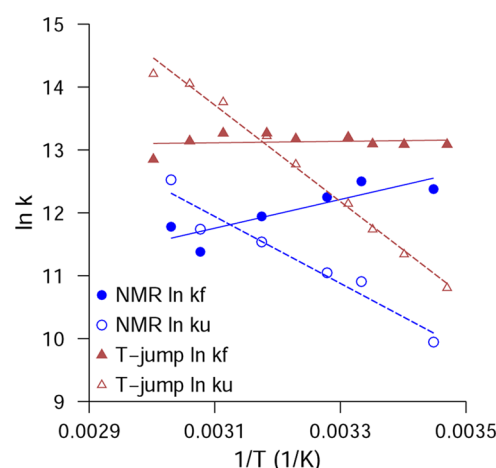

Figure 5. [P18A]-TC10b dynamics, an Arrhenius plot comparison, Trp fluorescence monitored T-jumps versus 18Hβ exchange broadening. From the least-squares fit line of the NMR dynamics data, $1/k_F$ = 4.8 μs at 300 K.

width *and* the %-dip are reproduced. The Δ^{ex} values from those two simulations are given by $\Delta^{sim} - \Delta^\circ$, with Δ° as the average intrinsic broadening of the reference methyl signals. This provides four measures of Δ^{ex}; the average value is employed in eq 1. With ln k_F values in the 12−14 range, the typical errors in ln k_F are ±0.18, and the largest errors observed were ±0.38.

Fluorescence-Monitored T-Jump Data. The experiments were performed at the University of Florida using an apparatus and methodology that has been described in detail previously.[25] Briefly, protein was dissolved at concentrations 20−30 μM in 50 mM phosphate buffer (pH 7) and then flowed through a silica capillary. Counter-propagating infrared laser pulses then induce a rapid (within <30 ns) but transient temperature increase of typically 6−8 °C, which triggers unfolding of the protein in a single-exponential process as monitored by tryptophan fluorescence. Fitting the exponential process to a two-state kinetic model that employs the equilibrium folding free energy determined from CD spectroscopy, we obtain the characteristic folding and unfolding rates shown in Figures 4 and 5.

Mutational $\Delta\Delta G$ and Φ_F Values. The data appearing in Table 1 provide multiple determinations for a number of single site mutations and for acidification (pH 2.5 stabilities versus those at pH 7). We designate the acidification effect as ΔpH: ΔpH = 3.13 ± 0.61 kJ/mol (over 10 observed cases). Three single site mutation effects, all fold-destabilizing, are also observed in three or more instances: Δ(S14A) = 5.55 ± 0.43 (n = 3), Δ(R16nva) = 5.5 ± 1.6 (n = 4), and Δ(P17A) = 2.37 ± 0.46 kJ/mol (n = 3). All of these are based on the ΔG_U^{300K} values in Table 1. A P12W mutation was also examined in multiple situations ($\Delta\Delta G_U^{mut}$ = −1.7 − +2.9 kJ/mol); no single value can be given for this mutation, vide infra.

The mutational (or acidification) Φ_F values are calculated at 300−305 K as

$$\Phi_F = 2.5[\ln(k_F^{mut}/k_F^{ref})](\Delta\Delta G_U^{mut})^{-1}$$

The calculation was repeated using the high and low estimates of the folding rates and with both the consensus $\Delta\Delta G_U$ value and the specific one for the system under study if the latter was available. This defined the range of values allowed for Φ_F.

RESULTS AND DISCUSSION

The original hallmark for folding dynamics in our laboratory, the broadening of the far upfield G11Hα2 signal, has been employed for additional dynamics measures. There are numerous potential pitfalls in the quantitative use of this probe: the signal is a doublet of doublets of doublets in H_2O and the coupling constants likely change as the unfolded state population increases on warming. In addition, the "unfolded" reference shift value cannot be equated with the random coil shift for Gly-Hα due to half-cage contributions in the "unfolded" state. These difficulties are reflected by reduced precision and accuracy in Arrhenius plots based on line broadening of this probe (Figure 4, vide infra).

To allow the observations of both the extremely shifted Gly-Hα2 and less shifted Hα3 resonance throughout a melt in ¹³C-edited 1D spectra, a series of ¹³Cα-Gly-11 labeled (G*) peptides were prepared: **X**-YAQWLKDG-G*-PSSGRPPPS (**X** = DA-, GA-, and N-). The **X** = DA species is TC10b. The two other species (**X** = GA- and N-, TC11b1, and TC12b) have also been previously characterized by NMR and CD studies;[8] the stability data appear in Table 1. The ¹³C-edited 1D spectra for ¹³Cα-TC10b appear as panel A of Figure 2. A number of alternative analyses for extracting dynamics data were examined.[22] For the final analyses, we chose to model the expectation "unfolded state" shifts as the temperature-dependent shifts for the Gly11-CH_2 of NAUYUQ-WLKDG-Gly11-PSSGRPAA. This analogue forms the complete cage structure only to a slight extent: χ_{cage} = 0.1 at 298 K (see Materials and Methods) since it lacks the terminal hydrophobic staple, the Y3/P19 interaction.

The NMR dynamics method with this probe, based on the line widths shown in part on panel A of Figure 2, provided a less than optimal Arrhenius plot even with the calibration of "unfolded" G11α2 shifts provided by the half-cage ensemble (Figure 4). The wide variance at the higher temperatures likely reflects errors in coupling constant estimates becoming a larger portion of the net broadening at the higher temperatures. The folding rate estimate at 300 K, a portion of the plot that was linear, was $1/k_F$ = 1.37 μs.

The dynamics for TC10b were also probed by fluorescence-monitored T-jump experiments. The resulting dynamics are

compared with the NMR data as Arrhenius plots in Figure 4. The two methods are, within experimental error, in agreement at the reference temperature. Our best estimate for $1/k_F$ at 298 K is 1.4 μs from this comparison. This is accord with the 1.5 μs value obtained by the Gai laboratory.[7]

Even though we still have some concerns about the validity of exchange-broadening at G11Hα2 as a probe, and the number of assumptions required in the analysis used to extract Δ^{ex}, we also report here the folding dynamics derived for the two other ^{13}C-Gly labeled analogues, TC11b1 and TC12b. These are given together with the data for TC10b in Table 2. For TC11b1 and TC12b, we employed the same analysis to arrive at both the Δ^{ex} value and unfolded ensemble shifts for the upfield shifted G11Hα.

Table 2. Folding Dynamics at 300 K for Trp-Cage Species with a [13]Cα Placed at Gly11

Trp cage analogue examined	χ_U	K_F	$1/k_F$ (μs)[a]	$1/k_U$ (μs)
TC10b (DAYA--)	0.140	6.14	1.43	8.8
TC11b1 (GAYA--)	0.296	2.37	4.4	10.4
TC12b (NYA--)	0.402	1.49	2.97	4.4
in 30 vol % TFE	0.181	4.53	2.55	11.5

[a]The folding rate for TC10b would be increased by a factor of 1.6 if the random coil shift for a Gly-Hα was employed instead of the estimated unfolded ensemble shift. The effects of choice of unfolded reference are much smaller (5−20%) for TC11b1 and TC12b.

The slower folding noted for TC11b1 (versus TC10b) may reflect a folding transition which includes the extension of the helix to the N-terminus of the sequence in which case the lack of an efficient N-cap in the GAYA- sequence could increase the barrier. The Φ_F value for the D1G mutation is 1.26, based on the data in Table 2. The faster folding observed for TC12b (versus TC11b1), even though the fold is further destabilized by helix truncation is puzzling; it can, however, be rationalized if helix N-capping has a greater impact on the folding barrier than on fold stability. In this regard it should be noted that the greater fold stability observed for TC12b in 30% TFE, presumably due to helix stabilization in this medium, is not reflected in a much more rapid folding rate; rather the stability appears to represent retarded unfolding upon the addition of the fold stabilizing cosolvent.

We have continued to monitor G11Hα2 line widths in our studies of Trp-cage unfolding, but the potential problems associated with this signal, particularly the questions concerning the temperature dependence of the chemical shift in the "unfolded ensemble", have led us to view this as a less than ideal measure of complete fold formation. In contrast, the large upfield shifts at the P18Hα (CSD = −2.33) and P18Hβ3 (CSD = −2.14 ppm, at 280 K), based on the shifts observed in a hyperstable cyclic construct[14,23] appeared to be superior measures of full cage formation. These appear only on complete cage formation; the P18Hα signal is usually overlapped with other peaks, but the P18Hβ3 signal appears far upfield with no other signals nearby. Were it not for its complex coupling, it would be an ideal NMR dynamics probe. Both signals are observed in the 2D NMR data of all analogues, and the derived CSDs provide χ_{cage} measures (typically in agreement to ±0.02) and the ΔG_U data shown in Table 1.

We reported the effects of individual Pro to Ala mutations on Trp-cage stability in 2008.[8] As previously noted the P19A mutation had the most profound destabilizing effect; the other

mutations were only slightly destabilizing. Of these, the [P18A] mutation introduces a far upfield doublet (typically in the 0.2− 0.8 ppm spectral window even on partial melting), an ideal situation for applying the line width difference method for deriving folding dynamics first reported by Olsen et al.[20] The 100%-folded CSD for the A18α signal of our most stable analogue is −2.7 ppm. That this value is slightly larger than the P18α structuring shift likely reflects a tighter packing onto the W6 indole ring that is allowed when the steric clashes of the C_γ methylene of the proline are absent. Of particular significance, any unfolded species in which the A18 methyl is not docked over the indole ring of the central Trp, including half-cage species, would display random coil shifts for both the β and α sites of Ala18. As a result, the [P18A]-Trp-cage mutants provide both a dynamics probe and a means for evaluating the ΔG_U of the full cage structure.

The [P18A] mutant of TC10b was examined by both NMR relaxation (line width measurements) and fluorescence-monitored T-jump experiments in 2005. The Arrhenius plots that resulted from these two studies appear in Figure 5. Upon comparison with the T-jump studies in Figure 4, it is clear that the [P18A] mutation ($\Delta\Delta G_U^{300} \approx -1.05$ kJ/mol; see Table 1) effects a retardation of the folding rate ($\Phi_F \approx 0.8$), particularly at the higher temperatures. The mutation significantly reduces the slope of the T-jump folding Arrhenius plot.

In the case of [P18A]-TC10b, however, the agreement between the fluorescence monitored T-jump and NMR determination of folding dynamics was very poor even after taking into account the greater error in the NMR determinations. In the ln k units shown in Figure 5, the errors ranged from ±0.14 to ±0.34 in the NMR dynamics experiment, versus a typical value of ±0.07 for the T-jump data points.

The NMR dynamics analysis based on A18β line widths (with the other Me doublets providing the measure of intrinsic broadening for the system) gave a folding Arrhenius plot with a distinctly positive slope. In addition, the NMR relaxation method afforded rates that were 2−3-fold slower; this was not fully rationalized and the basis for not publishing the results at that time.

Another distinction in Arrhenius plot comparison is the difference in apparent T_m by fluorescence versus the NMR measures. If we recalculate k_F and k_U values from the T-jump relaxation rates using the fraction folded values derived from the A18β signal NMR melt, the rate discrepancy remains. Since we viewed the upfield methyl signal of [P18A] Trp-cage mutants as a nearly ideal NMR dynamics probe, we have repeated a study of [P18A]-TC10b with freshly prepared material and using more precise line fitting procedures which we developed in other studies.[21] In this second determination, we once again obtained a positive Arrhenius folding plot slope with $1/k_F = 3.7$ μs at 300 K.

We now suggest a rationale: that many stable Trp-cage species have partially folded states, with cage formation still incomplete, that are both as helical as the native state *and* place the Trp indole in an environment that quenches its fluorescence. Thus, both the fluorescence measures and prior Trp-cage dynamics measures based on helical IR signals may not be probes of complete cage formation. We employed [P18A]-Trp-cages for our remaining studies, with the exchange line broadening at Ala18-Hβ as the dynamics probe.

We first examined the possibility of extending this method to an ultrastable Trp-cage system,[11] TC16b (DAYAQ WLKD**a** GPSS**a** RPPPS). If we assume the folding rate increase for

G10a observed for TC10b by Culik et al.[12] applies here as well, this would put the estimated rate for TC16b at 300 K at $1/k_F$ = 0.65−0.85 μs. [P18A]-TC16b, with a T_m of 76 °C at pH 7, did not display enough exchange broadening to yield a useful Arrhenius plot. However, with the fold destabilization observed at pH 2.5 ($\Delta\Delta G_U\Delta^{pH}$ = −3.1 kJ/mol, Table 1), useful data could be collected; again a positive slope was observed (from 305−320 K) with $1/k_F$ = 0.93 ± 0.18 μs at 305 K (Figure S1, Supporting Information (SI)). This fast folding rate, under conditions where the salt bridge is removed by aspartate protonation, suggests that the salt bridge is not a required feature for accelerated cage formation.

We also collected dynamics data for the [P17A,P18A] mutant of TC16b at pH 2.5 (Figure S2, SI). Over the 285−315 K range, a positive Arrhenius slope was observed with a $1/k_F$ = 2.20 ± 0.19 μs at 305 K. The Φ_F value calculated for the P17A mutation was ca. 0.85 at the 305 K comparison point. We attribute the folding rate retardation of the [P17A]-mutation, in combination with P18A, to destabilization of the polyPro$_{II}$ conformation in the C-terminal segment. This conformation is required for proper docking against Y3 and W6 in cage formation and is reflected in the near unity Φ_F value for the [P17A] and [P18A] mutations.

More dramatic destabilizations were required to obtain data at pH 7. An Arg16 to norvaline mutation proved suitable.

This mutation, by removing the entire guanidine-group, eliminates both the H-bonding and Coulombic components of the D9/R16 salt bridge. The $\Delta\Delta G_U$ values for [R16nva] mutations are comparable to, or significantly larger, than those due to acidification (see Table 1). This mutation, in combination with the [P18A] mutation, allowed dynamics studies at pH 7. The [R16nva, P18A]-TC16b analogue gave excellent data which yielded a slightly curved Arrhenius plot for ln k_F (Figure 6). Similarly curved Arrhenius plots are typically
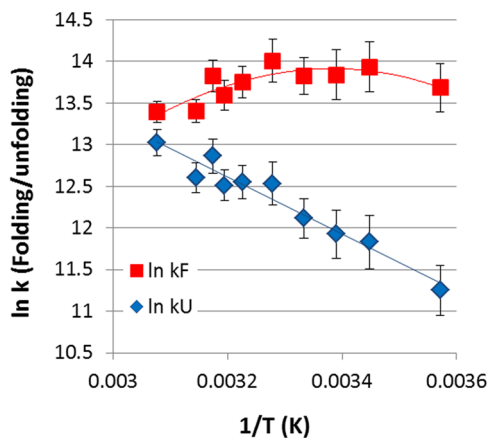

Figure 6. Folding dynamics of [R16nva,P18A]-TC16b at pH 7.

observed for small protein folds.[26] The maximum rate, $1/k_F$ = 0.95 ± 0.10 μs, was observed between 290−305 K. Since we do not have data for [P18A]-TC16b at pH 7, we cannot calculate a Φ_F value (see SI, note 1). This observation also suggests that salt-bridge formation does not occur until after the folding transition state.

We next turned to examination of the C-terminal segment of the helix in the Trp-cage. Studies already presented above indicated that helix N-capping appears to be required in a transition state leading to structures that provided the full ring

current shielding of Gly11 Hα2. The greater fold stability of TC10b and TC13b (versus TC5b) is attributable to improvements in helicity. As already noted,[27] in prior dynamics studies relying on IR probes, helicity improvements resulted in folding acceleration, with a near unity Φ_F value. We opted to examine a destabilizing mutation at the C-terminus of the helix, A8G, to obtain another helicity-associated Φ_F value. From Table 1, this substitution results in a 4.1 kJ/mol cage fold destabilization at 300 K. For this species, [A8G,P18A]-TC16b, with χ_U values greater than 0.1 at all temperatures above 300 K at both pH 2.5 and 7, dynamics data could be obtained at both pH 7 and 2.5. The resulting Arrhenius plots appear in Figure 7.
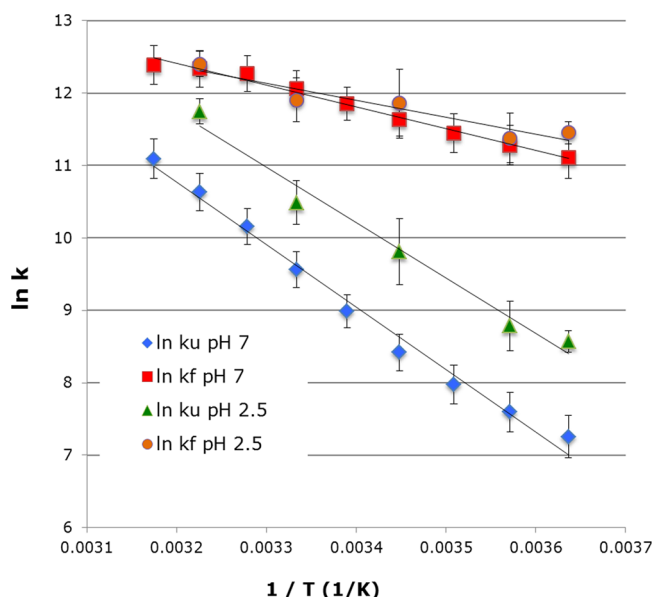

Figure 7. Folding/unfolding Arrhenius plots for [A8G,P18A]-TC16b at pH 7 and pH 2.5.

Since we were able to obtain dynamics data for [P18A]-TC16b at pH 2.5, the comparison at this pH provides a direct measure of the Φ_F value for the A8G mutation. The folding time constant at the 305 K comparison point is 5.1 μs for [A8G,P18A]-TC16b, which corresponds to Φ_F = 1.19 ± 0.08. Essentially the same value would be obtained at pH 7 using the extrapolated[27] folding time constant for [P18A]-TC16b.

This example also provides the first example of a direct folding dynamics comparison at pH 7 versus pH 2.5. In Figure 7, the Arrhenius plots for folding are, within experimental error, identical at the two pH's. The enhanced fold stability at pH 7 is exclusively the result of a decreased unfolding rate. The favorable Coulombic attraction associated with the D9/R16 salt bridge is present in the folded state but essentially gone at the unfolding/folding transition state.

The most destabilizing single site mutation for the Trp-cage, other than P19A and Y3A, is the S14A mutation. The basis for this is now established.[14,23,27] In all cases, H$_\gamma$ of the serine hydroxyl forms an H-bond to O=C-Gly11. In the crystal structure[23] of a cyclic Trp-cage that lacks the R16/D9 salt bridge due to the pH employed for crystallization, the S14H$_\gamma$/ O=C-Gly11 interaction is clearly present and the Ser-O$_\gamma$ accepts an H-bond from R16H$_N$ (the amide NH). In analogues with an R16/D9 salt-bridge, the Arg side chain wrapping around the indole ring places R16Hε, a side chain NH, in position for H-bonding to Ser-O$_\gamma$ either directly or via a tightly

associated water molecule.[23,27a] These H-bonding interactions are required to allow the burial of the polar S14 side chain in the hydrophobic core, and they contribute a net stabilization of the cage fold. As a result, even though the introduction of an additional alanine in the 3_{10} helix might be expected to provide some net stabilization to this secondary structure element, an S14A mutation is fold-destabilizing ($\Delta\Delta G_U = -5.5 \pm 0.4$ kJ/mol). The dynamics effects of the S14A mutation were examined for [S14A,P18A]-TC16b. For this system, the $\Delta\Delta G_U$ for the [S14A]-mutation was −5.3 kJ/mol at both pH 7 and pH 2.5, but the dynamics probe was free of interfering peak overlaps only at pH 7. [S14A,P18A]-TC16b displayed a nearly constant folding rate ($1/k_F = 1.73 \pm 0.15$ μs) in the 295−320 K temperature span (Figure 9, vide infra). Since we could not obtain dynamics data for [P18A]-TC16b at pH 7, a direct comparison for a Φ_F calculation does not exist (see SI, note 2). The slightly more stable [A8G,P18A]-TC16b analogue, which has a comparable fold stability (ΔG_U 1.2 kJ/mol greater than that of [S14A,P18A]-TC16b), provides the best comparison point. The folding time constants are 5.1 and 1.73 μs, respectively, for [A8G,P18A]-TC16b and [S14A,P18A]-TC16b: the [S14A] mutant folds faster than the more stable [A8G] mutant. From this comparison, it is clear that the [S14A] mutation does not result in the dramatic folding rate reduction that might be expected for such a destabilizing effect. If the S14 side chain is already buried at the folding transition state, the web of stabilizing side chain H-bonding interactions is not fully established. No matter how we estimate it, Φ_F is much less than 0.5 for the [S14A] mutation.

Other than replacing long chain residues with alanine in helices[8,9] and the Gly to D-Ala mutations[11,12] in the C-terminal cap of the Trp-cage's N-terminal helix, a [P12W] mutation[13,14] is the most fold stabilizing mutation reported for the Trp-cage. In the case of TC5b, this mutation has been reported to have a stabilizing effect (a positive ΔT_m by CD) and provides a significantly greater acceleration of the folding rate.[7] This published account indicates a Φ_F in excess of 1.2. The same ΔT_m for a [P12W] mutation has also been observed for TC16b and a circularly permuted Trp-cage sequence and $\Delta\Delta G_U$ values on the order of +2 to +3 kJ/mol were derived[14] for this mutation. The data in Table 1 indicate that a [P12W] mutation is not fold stabilizing for Trp-cages with the Pro18 to Ala mutation, $\Delta\Delta G_U^{P12W}$ values at 300 K are −2.4 (for [P18A]-TC10b), −1.3 (for [P18A]-TC16b), and −1.7 kJ (for [S14A,P18A]-TC16b).

Two explanations for the fold stabilizing effect of the [P12W]-mutation in Trp-cage structures have been suggested: the formation of an enthalpically favorable edge-to-face (EtF) indole/indole cluster,[13] and greater apolar surface burial[14] associated with the W12/P17,18 as well as the W12/W6 interactions; see Figure 8. Both of these may apply in the case of Trp-cages that retain the C-terminal tri-Pro unit, but the relative extent to which they affect energies of the folding transition state and the final folded structure are not known.

In the case of TC5b, rate comparisons[7,13] suggest that the [P12W] mutation may have a greater stabilizing effect on the folding transition state, $\Phi_F \geq 1.2$. We examined the dynamics of [P12W]-Trp-cages in two species, both of which also had the [P18A] mutation that provides our preferred dynamics probe. Although an indole/indole aryl cluster could still be a feature of the folding transition state, with a [P18A] mutation in place, the extent of apolar surface burial resulting is significantly diminished (Figure 8). This is our rationale for the observation
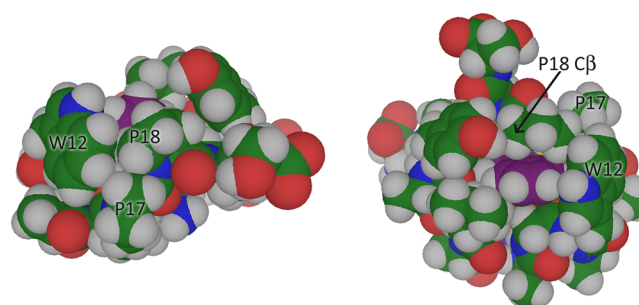

Figure 8. Views of the packing interactions of W12 in a Trp2-cage taken from a previously reported[14] structure, W6 appears in magenta. The left panel shows the close contacts between the edge of the indole ring and the P17Cβ and P18Cδ methylenes. The right panel shows the edge-to-face interaction between the two indole rings and the location of P18Cβ which is the only aliphatic unit retained in the P18A mutants. The hydrophobic cluster consisting of the W12 indole ring edge and the P17/P18 interface is significantly disrupted by the [P18A] mutation.

that the [P12W] mutation was a fold-destabilizing rather than stabilizing effect when the [P18A] mutation was present. In the case of [P12W,P18A]-TC13b, the net effect of the double mutation was a 1.1 kJ/mol destabilization; the addition of the [P18A] mutation to [P12W]-TC13b corresponded to a 4 kJ/mol loss in fold stability. The folding time constants observed for [P12W,P18A]-TC13b were quite rapid (see Figure S3, SI), with a positive slope for the ln k_F versus $1/T$ plot: $1/k_F = 1.5 \pm 0.15$ μs (at 305 K) and 0.9 ± 0.2 μs (at 295 K). However, the slope of the Arrhenius plot for unfolding was significantly less steep than those observed for other [P18A]-Trp-cage species of comparable fold stability. Extrapolated k_F values from other [P18A]-Trp-cage species, based on Φ_F values for substitutions in the helices, suggest that the [P12W] mutation provides a modest folding acceleration at the lower temperatures even though it has a net fold destabilizing effect, corresponding to a significant *negative* Φ_F value.

In the case of the other Trp2-cage examined in the present study, [P12W,S14A,P18A]-TC16b, a direct comparison is available (Figure 9). In this construct, the [P12W] mutation was destabilizing by 1.7 kJ/mol at 300 K (Table 1).

In this example we also observed a diminished slope for ln k_U vs $1/T$. The destabilization of the fold associated with the [P12W] mutation predominantly results from accelerated unfolding particularly at the lower temperatures. The loss of curvature in the folding Arrhenius plot presumably reflects a
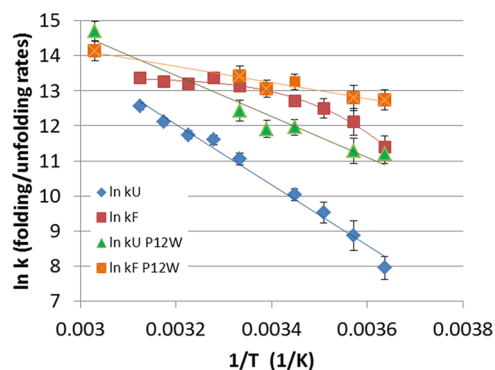

Figure 9. Arrhenius plots of the folding dynamics of [S14A,P18A]-TC16b with and without the addition of a [P12W] mutation.

change in $\Delta C_p^{\ddagger}$ and signals a change in apolar surface burial at the transition state. Finally, at the lowest temperatures there is a significant increase, at least 2.2-fold (4.1 ± 1.9), in the folding rate associated with the [P12W] mutation. This places the Φ_F value for the [P12W] mutation in the range of -0.7 to -1.0 at 275 K.

■ CONCLUSIONS

Fold stability data are reported for 14 new Trp-cage species, some at both acidic and neutral pH values. These systems include a number of cases in which the circular dichroism (which detects only net helicity) provides higher T_m's and measures of folded population (χ_F) than chemical shifts that report on formation of the complete cage structure. These observations indicate partial structuring without full cage formation in a number of species with either compromised cage features or mutations that enhance intrinsic helicity.[8,9] The single site mutations that resulted in the largest decreases in cage formation, with much less effect on helix formation, were P19A ≫ S14A > P17A > R16nva. Since our interest lay in examining the rates at which the full cage motif forms, we chose chemical shift melts at residue 18 sites as the measure for obtaining a set of fold stability measures (as ΔG_U at 300 K, Table 1) for both the new analogues and prior reference constructs: these reflect complete cage formation. Previously noted mutational effects on cage stability were, with one exception, confirmed by these new measures of folded fractions. The exception was the P12W mutation; the new analogues included instances where a P12W mutation was fold destabilizing rather than fold stabilizing as was the case in both the original instance[13] and more recent[14] studies.

Many of the new analogues bear a [P18A] mutation, which is, in the absence of a [P12W] mutation, fold-destabilizing by only 1.2 kJ/mol. The exchange broadening of the methyl resonance of the alanine introduced in place of P18 served as our primary NMR dynamics probe. This method of folding dynamics analysis requires the observation of exchange broadening due to the equilibrium between the fully folded state and states that have P18A undocked from Trp6 and thus lack the 1.13−1.19 upfield ring current shift at 18Hβ. A pseudo-two-state assumption was applied to derive the fold populations essential for the extraction of k_F and k_U values. We assume that the equilibrium fraction of the "unfolded state ensemble" can be derived from the observed chemical shift of a probe, taking it as a population weighted average of the random coil value and the fully folded value. If other states with different chemical shifts were populated, this analysis would be incorrect and this would be apparent in non-Arrhenius behavior for the derived folding/unfolding rate constants. In other applications of this dynamics analysis method,[21,36] we have observed dramatic slope changes in Arrhenius plots and disagreement in rates derived by probes placed in different sites for systems with more complicated folding scenarios. The strict Arrhenius behavior seen in Figures 6, 7, 9 and in the supporting figures, thus serves as a confirmation of two-state behavior for the final docking event that provides the native fold.

The inherent limitation of the NMR dynamics method prevented the determination of folding rates for some of the most stable Trp-cage analogues that have been prepared. The extent of line broadening was insufficient for species with $1/k_F$ values greater than 0.7 μs and in cases where a "P18A undocked from Trp6" state does not become populated ($\chi_U \geq 0.08$) at temperatures below 310 K. In some cases, dynamics were

measured at pH 2.5 to take advantage of the fold destabilizing effect of Asp1,9 protonation ($\Delta\Delta G = 3.1$ kJ/mol) to increase the unfolded state population and thus increases the extent of exchange broadening that can be observed providing folding rate constants with greater precision. Ten [P18A]-Trp-cage species have been examined at either pH 2.5 or pH 7, one of them at both pH values.

All of our data indicate that the N-terminal helix (residues 1−8) is fully formed at the cage folding transition state. This is consistent with a number of recent MD simulations.[1c,27b,28,29] The Φ_F value for an [A8G] mutation was 1.19 ± 0.08 and similar, slightly in excess of unity, Φ_F values are implied by the systematic increases in folding rate constants for Trp-cages with additional alanine residues in the N-terminal helix based both on the present study and a prior published account.[7] A more limited study of exchange broadening at the upfield shifted G11Hα2 in the present study indicated that more effective N-capping residues at the first position of this helix also accelerate folding. The importance of the N-capping interaction has also been supported by a recent dynamics study.[30] Near unity Φ_F values were also found for the [P17A] and (to the extent that we can approximate it) the [P18A] mutations. The simplest rationale for these is that docking of the P17−P19 unit onto the Trp-bearing helix is favored when this unit has a high preference for the poly-Pro$_{II}$ conformation that is present in the fully folded state.

In contrast to this, we observe negative Φ_F values for the P12W mutation when the P18A mutation is also present, and small fractional Φ_F values were observed for ionization state changes and the R16nva and S14A mutations. The near absence of folding rate retardation due to the R16nva mutation and protonation of the Asp in the D9/R16 salt bridge indicates that the fold-stabilizing D9/R16 interaction ($\Delta\Delta G_U \approx -5$ kJ/mol) forms after the cage formation transition state. Gai and co-worker have reached the same conclusion, based on an R16K mutation.[7] This conclusion, post-transition state formation, was also extended this to the P19/Y3 hydrophobic staple. In our view the latter point requires further study using cage-specific probes, and efforts in this direction are in progress. A recent transition state interface sampling modified Markov State Model[31] finds breaking of the salt-bridge as a very early event in the unfolding trajectory, well prior to any loss of helicity. However, premature salt bridge formation continues[32] to appear as a kinetic trap in folding simulations.

The S14A mutation has a dramatic destabilizing effect on the cage fold ($\Delta\Delta G_U = -5.6$ kJ/mol) and is located in the 3$_{10}$ helical segment of the Trp-cage. This structural element has been a subject of discussion in MD simulations,[2,28,32] and experimental evidence for residual flexibility at this site has been reported based on both NMR structure ensembles[8,14,19,33] and crystal structures.[23] Gai and co-workers[7] have observed a more rapid phase (ca. 300 ns) in some FT-IR-monitored T-jump experiments which was attributed to the 3$_{10}$ helix. Two experimental reports that have implicated an intermediate state populated at temperatures near the apparent T_m have also focused on the G11-G15 segment. Ahmed et al.[34] indicated that this structure was more compact with closer contacts about W6, but a less well-formed 3$_{10}$ helix. Rovo et al.[33] have calculated that this intermediate has a longer, nearly complete, α-helix in the G11-G15 segment. Whether this intermediate, which appears to be most populated at somewhat higher temperatures, is an on-path folding intermediate at these or lower temperatures, is unclear. If some compact intermediate is on-

path, one possibility is that the H-bonding interactions that allow burial of the S14 side chain hydroxyl form after the P17−P19 docking event and are the basis for the late conformational change in the G11-G15 segment. D9/R16 salt-bridge formation may also contribute to this conformational change.

P12 is also within the 3_{10} helical segment of the Trp-cage. While further data, including dynamics for [P12W]-species that retain the P17,18,19 unit based on NMR probes within that unit, are required to fully clarify the nature of the contacts made by Trp12 in the folding transition state, the present study does provide insights. The rapid folding of [P12W,P18A]-species implies some fold-favoring interactions at Trp12. Partial formation of a Trp6/Trp12 aryl ring cluster at the transition state may be the rationale for folding that is more rapid, even though the [P12W] mutation is destabilizing in the ultimate folded state. Such a propensity to form an indole/indole cluster in the unfolded state ensemble could favor prestructuring at the transition state. This local structure may, however, differ from that in the final folded state with, in the case of the [P18A]-analogues, favorable interactions present only at the folding transition state. Our analysis suggests that with a proline present at position 18, additional hydrophobic interactions that are not present in [P18A] analogues, result upon full cage formation and provide stabilization of the fully folded state.

While there are unanswered questions concerning the Trp-cage folding pathway, with a number of groups having reported data suggesting that Trp-cage folding is not a two-state system,[19,28,33−35] these data are largely associated with structure melting analysis rather dynamics measurements. Both T-jump and NMR relaxation experiments are consistent with a net two-state process, with fewer exceptions.[7,28] With the present study, it is apparent that mutations that increase the propensity to form any of the local secondary structure features of the Trp-cage fold produce folding rate increases, likely due to partial or complete structuring of these units prior to the ultimate folding transition state. In more stable Trp-cage sequences, there may be considerable folding trajectory variability: concerted formation of the full cage structure from an unfolded state ensemble when the N-terminal helix is not intrinsically favorable versus partial, variable degrees of prestructuring of the individual secondary structure elements (most notably the N-terminal helix, but also the poly-Pro$_{II}$ segment and possibly half-cage species). The NMR dynamics method employed herein affords the slowest time constant involved in an equilibrium between two states of a probe that have a large chemical shift difference. By employing a site with ring current shifts that only appear on complete docking of residues 17−19 upon the Trp/Tyr-bearing helix focuses our study on the, presumably late, cage-forming step. The Arrhenius plots for folding that result imply a significant barrier, and we continue to view this ultimate step in the formation of Trp-cage as effectively a two-state process.

ASSOCIATED CONTENT

⑤ Supporting Information
Folding and unfolding data (as Arrhenius plots) for [P18A]-TC16b and [P17A,P18A]-TC16b at pH 2.5, and [P12W,P18A]-TC13b at pH 7. This material is available free of charge via the Internet at http://pubs.acs.org.

AUTHOR INFORMATION

Corresponding Author
*E-mail: andersen@chem.washington.edu.

Notes
The authors declare no competing financial interest.

■ REFERENCES

(1) (a) Searle, M. S., and Ciani, B. (2004) Design of β-sheet systems for understanding the thermodynamics and kinetics of protein folding. *Curr. Opin. Struct. Biol. 14*, 458−464. (b) Ghosh, K., Ozkan, S. B., and Dill, K. A. (2007) The Ultimate Speed Limit to Protein Folding is Conformational Searching. *J. Am. Chem. Soc. 129*, 11920−11927. (c) Gelman, H., and Gruebele, M. (2014) Fast protein folding kinetics. *Q. Rev. Biophys. 47*, 95−142. (d) Lindorff-Larsen, K., Piana, S., Dror, R. O., and Shaw, D. E. (2011) How Fast-Folding Proteins Fold. *Science 334*, 517−520.

(2) Day, R., Paschek, D., and Garcia, A. E. (2010) Microsecond simulations of the folding/unfolding thermodynamics of the Trp-cage miniprotein. *Proteins 78*, 1889−1899 and references cited therein.

(3) Andersen, N. H., Fesinmeyer, R. M., Neidigh, J. W., and Barua, B. (2001) The Trp-Cage: A Notably Stable Mini-Protein Fold. *Peptides 2000: Proceedings of the 26th European Peptide Symposium* (Martinez, J., Fehrentz, J.-A., Eds.) pp 45−46, EDK, Paris, France.

(4) Neidigh, J. W., Fesinmeyer, R. M., and Andersen, N. H. (2002) Designing a 20-Residue Protein. *Nat. Struct. Biol. 9*, 425−430.

(5) McMillan, A. W., Kier, B. L., Shu, I, Byrne, A., Andersen, N. H., and Parson, W. W. (2013) Fluorescence of Tryptophan in Designed Hairpin and Trp-cage Miniproteins: Measurements of Fluorescence Yields and Calculations by Quantum Mechanical Molecular Dynamics Simulations. *J. Phys. Chem. B 117*, 1790−1809.

(6) Qiu, L., Pabit, S. A., Roitberg, A. E., and Hagen, S. J. (2002) Smaller and Faster: The 20-Residue Trp-Cage Protein Folds in 4 μs. *J. Am. Chem. Soc. 124*, 12952−12953.

(7) Culik, R. M., Serrano, A. L., Bunagan, M. R., and Gai, F. (2011) Achieving Secondary Structural Resolution in Kinetic Measurements of Protein Folding: A Case Study of the Folding Mechanism of Trp-cage. *Angew. Chem., Int. Ed. 50*, 10884−10887.

(8) Barua, B., Lin, J. C., Williams, D. V., Neidigh, J. W., Kummler, P., and Andersen, N. H. (2008) The Trp-cage: Optimizing the Stability of a Globular Miniprotein. *Prot. Eng. Des. Sel. 21*, 171−185.

(9) Lin, J. C., Barua, B., and Andersen, N. H. (2004) The Helical Alanine Controversy: An (Ala)$_6$ Insertion Dramatically Increases Helicity. *J. Am. Chem. Soc. 126*, 13679−13684.

(10) Werner, J. H., Dyer, R. B., Fesinmeyer, R. M., and Andersen, N. H. (2002) Dynamics of the Primary Processes of Protein Folding: Helix Nucleation. *J. Phys. Chem. B 106*, 487−494.

(11) Williams, D. V., Barua, B., and Andersen, N. H. (2008) Hyperstable Miniproteins: Additive Effects of D- and L-Ala Mutations. *Org. Biomol. Chem. 6*, 4287−4289.

(12) Culik, R. M., Annavarapu, S., and Nanda, V. (2013) Using D-amino acids to delineate the mechanism of protein folding: Application to Trp-cage. *Chem. Phys.*, 131−134.

(13) Bunagan, M. R., Yang, X., Saven, J. G., and Gai, F. (2006) Ultrafast Folding of a Computationally Designed Trp-Cage Mutant: Trp2-Cage. *J. Phys. Chem. B 110*, 3759−3763.

(14) Byrne, A., Kier, B. L., Williams, D. V., Scian, M., and Andersen, N. H. (2013) Circular Permutation of the Trp-cage: Fold Rescue upon Addition of a Hydrophobic Staple. *RSC Adv. 3*, 19824−19829.

(15) Williams, D. V., Byrne, A., Stewart, J. M., and Andersen, N. H. (2011) Concerning the Optimal Salt Bridge for Trp-cage Stabilization. *Biochemistry 50*, 1143−1152.

(16) Early on-path helix formation has also been observed in MD folding simulations: (a) Juraszek, J., and Bolhuis, P. G. (2006) Sampling the multiple folding mechanisms of Trp-cage in explicit solvent. *Proc. Natl. Acad. Sci. U.S.A. 103*, 15859−15864. (b) Xu, W., and Mu, Y. (2008) Ab initio Folding Simulation of Trpcage by Replica Exchange with Hybrid Hamiltonian. *Biophys. Chem. 137*, 116−125.

(17) Mok, K. H., Kuhn, L. T., Goez, M., Day, I. J., Lin, J. C., Andersen, N. H., and Hore, P. J. (2007) A pre-existing hydrophobic collapse in the unfolded state of an ultrafast folding protein. *Nature* 447, 106−109.

(18) Neidigh, J. W., and Andersen, N. H. (2002) Peptide Conformational Changes Induced by Tryptophan-Phosphocholine Interactions in a Micelle. *Biopolymers* 65, 354−361.

(19) Hałabis, A., Żmudzińska, W., Liwo, A., and Ołdziej, S. (2012) Conformational Dynamics of the Trp-Cage Miniprotein at Its Folding Temperature. *J. Phys. Chem. B* 116, 6898−6907.

(20) Olsen, K. A., Fesinmeyer, R. M., Stewart, J., and Andersen, N. H. (2005) Hairpin folding rates reflect mutations within and remote from the turn region. *Proc. Natl. Acad. Sci. U.S.A.* 102, 15483−15487.

(21) Scian, M., Shu, I., Olsen, K. A., Hassam, K., and Andersen, N. H. (2013) Mutational Effects on the Folding Dynamics of a Minimized Hairpin. *Biochemistry* 52, 2556−2564.

(22) Barua, B. (2005) Design and Study of Trp-cage Miniproteins: Chemical Shift Tools in Peptide Folding and Miniature Protein Design, Ph.D. thesis, Chemistry Department, University of Washington, Seattle, USA, pp 50−65.

(23) Scian, M., Lin, J. C., Le Trong, I., Makhatadze, G. I., Stenkamp, R. E., and Andersen, N. H. (2012) Crystal and NMR structures of a Trp-cage mini-protein benchmark for computational fold prediction. *Proc. Natl. Acad. Sci. U.S.A.* 109, 12521−12525.

(24) Piette, L. H., and Anderson, W. A. (1959) Potential Energy Barrier Determinations for Some Alkyl Nitrites by Nuclear Magnetic Resonance. *J. Chem. Phys.* 30, 899−908.

(25) Hagen, S. J. (2012) Laser temperature-jump spectroscopy of intrinsically disordered proteins. *Methods Mol. Biol.* 896, 267−81.

(26) (a) Nguyen, H., Jäger, M., Kelly, J. W., and Gruebele, M. (2005) Engineering a beta-Sheet Protein toward the Folding Speed Limit. *J. Phys. Chem. B* 109, 15182−15186. (b) Luo, L., and Lu, J. (2011) Temperature Dependence of Protein Folding Deduced from Quantum Transition. *Quant. Biol. Biomol.*, arXiv:1102.3748. (c) Karplus, M. (2000) Aspects of Protein Reaction Dynamics: Deviations from Simple Behavior. *J. Phys. Chem. B* 104, 11−27. (d) Ferrara, P., Apostolakis, J., and Caflish, A. (2000) Thermodyanmics and Kinetics of Folding of Two Model Peptides Investigated by Molecular Dynamics Simulations. *J. Phys. Chem. B* 104, 5000−5010. (e) Crane, J. C., Koepf, E. K., Kelly, J. W., and Gruebele, M. (2000) Mapping the Transition State of the WW Domain β-Sheet. *J. Mol. Biol.* 298, 283−292. (f) Fuller, A. A., Du, D., Liu, F., Davoren, J. E., Bhabha, G., Kroon, G., Case, D. A., Dyson, H. J., Powers, E. T., Wipf, P., Gruebele, M., and Kelly, J. W. (2009) Evaluating β-turn mimics as β-sheet folding nucleators. *Proc. Natl. Acad. Sci. U.S.A.* 106, 11067−11072.

(27) (a) Paschek, D., Nymeyer, H., and García, A. E. (2007) Replica exchange simulation of reversible folding/unfolding of the Trp-cage miniprotein in explicit solvent: On the structure and possible role of internal water. *J. Struct. Biol.* 157, 524−533. (b) Paschek, D., Hempel, S., and Garcia, A. E. (2008) Computing the stability diagram of the Trp-cage miniprotein. *Proc. Natl. Acad. Sci. U.S.A.* 105, 17754−17759.

(28) Meuzelaar, H., Marino, K. A., Huerta-Viga, A., Panman, M. R., Smeenk, L. E. J., Kettelarij, A. J., van Maarseveen, J. H., Timmerman, P., Bolhuis, P. G., and Woutersen, S. (2013) Folding Dynamics of the Trp-Cage Miniprotein: Evidence for a Native-Like Intermediate from Combined Time-Resolved Vibrational Spectroscopy and Molecular Dynamics Simulations. *J. Phys. Chem. B* 117, 11490−11501.

(29) (a) Lee, I. H., and Kim, S. Y. (2013) Dynamic folding pathway models of the Trp-cage protein. *Biomed. Res. Int.* 2013, 973867. (b) Doshi, U., and Hamelberg, D. (2014) Achieving Rigorous Accelerated Conformational Sampling in Explicit Solvent. *Phys. Chem. Lett. 5*, 1217−1224.

(30) Markiewicz, B. N., Jo, H., Culik, R. M., DeGrado, W. F., and Gai, F. (2013) Assessment of Local Friction in Protein Folding Dynamics Using a Helix Cross-Linker. *J. Phys. Chem. B* 117, 14688−14696.

(31) Du, W., and Bolhuis, P. G. (2014) Sampling the equilibrium kinetic network of Trp-cage in explicit solvent. *J. Chem. Phys.* 140, 195102.

(32) Hu, Z., Tang, Y., Wang, H., Zhang, X., and Lei, M. (2008) Dynamics and cooperativity of Trp-cage folding. *Arch. Biochem. Biophys.* 475, 140−147.

(33) Rovó, P., Stráner, P., Láng, A., Bartha, I., Huszár, K., Nyitray, L., and Perczel, A. (2013) Structural Insights into the Trp-Cage Folding Intermediate Formation. *Chem.—Eur. J.* 19, 2628−2640.

(34) Ahmed, Z., Beta, I. A., Mikhonin, A. V., and Asher, S. A. (2005) UV-resonance raman thermal unfolding study of Trp-cage shows that it is not a simple two-state miniprotein. *J. Am. Chem. Soc.* 127, 10943−10950.

(35) Neuweiler, H., Doose, S., and Sauer, M. (2005) A microscopic view of miniprotein folding: Enhanced folding efficiency through formation of an intermediate. *Proc. Natl. Acad. Sci. U.S.A.* 102, 16650.

(36) (a) Kier, B. L., Anderson, J. M., and Andersen, N. H. (2014) Circular Permutation of a WW Domain: Folding Still Occurs after Excising the Turn of the Folding-Nucleating Hairpin. *J. Am. Chem. Soc.* 136, 741−749. (b) Dyer, R. B., Maness, S. J., Franzen, S., Fesinmeyer, R. M., Olsen, K. A., and Andersen, N. H. (2005) Hairpin Folding Dynamics: The Cold-denatured State is Predisposed for Rapid Refolding. *Biochemistry* 44, 10406−10415.